

Structure to Property: Chemical Element Embeddings and a Deep Learning Approach for Accurate Prediction of Chemical Properties

Shokirbek Shermukhamedov¹, Dilrom Mamurjonova² and Michael Probst^{1,3}

Abstract

The application of machine learning (ML) techniques in computational chemistry has led to significant advances in predicting molecular properties, accelerating drug discovery, and material design. ML models can extract hidden patterns and relationships from complex and large datasets, allowing for the prediction of various chemical properties with high accuracy. The use of such methods has enabled the discovery of molecules and materials that were previously difficult to identify. This paper introduces a new ML model based on deep learning techniques, such as a multilayer encoder and decoder architecture, for classification tasks. We demonstrate the opportunities offered by our approach by applying it to various types of input data, including organic and inorganic compounds. In particular, we developed and tested the model using the *Matbench* and *Moleculenet* benchmarks, which include crystal properties and drug design-related benchmarks. We also conduct a comprehensive analysis of vector representations of chemical compounds, shedding light on the underlying patterns in molecular data. The models used in this work exhibit a high degree of predictive power, underscoring the progress that can be made with refined machine learning when applied to molecular and material datasets. For instance, on the Tox21 dataset, we achieved an average accuracy of 96%, surpassing the previous best result by 10%. Our code is publicly available at <https://github.com/dmamur/elembert>.

1 Introduction

Due to their effectiveness in fitting experimental data and predicting material properties, machine learning models have found extensive applications in research on batteries^{1,2}, supercapacitors³, thermoelectric⁴ and photoelectric⁵ devices, catalysts⁶ and in drug design⁷. In a 'second wave', deep learning models (DLMs) have exhibited remarkable potential in advancing the field of chemical applications. So-called Word2vec⁸ DLMs have been used for processing chemical text data extracted from academic articles. By representing chemical formulas as embeddings or vectors, non-obvious connections between compounds and chemical properties can be discovered. For instance, the mat2vec⁹ NLP model was able to predict materials with good thermoelectric properties, even when these materials and their properties were not explicitly named in the original papers. Other NLP-inspired models, such as Bag of Bonds¹⁰, mol2vec¹¹, smile2vec¹², SPvec¹³, have used unsupervised machine learning and have been applied to chemical compound classification tasks, achieving remarkable results. These models hold immense potential for accelerating the discovery and the design of materials with tailored properties.

In this regard, the type of input data is crucial for ML models. In chemistry, this could be chemical text data, like in mat2vec, or structural data. Chemical texts make it possible to use reference information of a compound¹⁴, such as weight, melting point, crystallization temperature, and element composition. These types of inputs can, in turn, be used by general deep learning models, with ELMO, BERT, and GPT-3 (or GPT-4) being the most famous examples.

One of the most common types of input data used for ML-based approaches is structural representation, which provides valuable information about the atomic environment of a given material. However, text-based data does not normally capture important structural features, such as interatomic distances. Structural information is crucial for predicting material properties, as it is key to all pertinent physical and chemical characteristics. This can be understood in the same sense as the Born-Oppenheimer approximation, in short, states that atomic coordinates (and from them the potential energy) are all that is needed in chemistry. The challenge of linking structural information to material properties is commonly referred to as the "structure to property" task. Overcoming this challenge has the potential to greatly enhance our ability to predict and design novel materials with desired properties.

Structure could be translated into property by graph neural networks (GNN) or high-dimensional neural networks (HDNN) formalisms. GNNs transform graphs of molecules (or compounds) into node and edge embeddings, which can then be used for state-of-the-art tasks¹⁵⁻²¹. HDNNs based on converting Cartesian coordinates of atoms to continuous representations use techniques like the smooth overlap of atomic positions (SOAP)²², the many-body tensor representation (MBTR)²³, or the atomic centered symmetry functions (ACSF)²⁴ to achieve the same goal. Message passing neural networks (MPNN) are a subgroup of HDNN that use atomic positions and nuclear charges as input. Examples include SchNet²⁵ and PhysNet²⁶. In

¹Institute of Ion Physics and Applied Physics, University of Innsbruck, 6020 Innsbruck, Austria ²Tashkent Chemical Technological Institute, 100011 Tashkent, Uzbekistan ³School of Molecular Science and Engineering, Vidyasirimedhi Institute of Science and Technology, 21201 Rayong, Thailand. Correspondence to: Shokirbek Shermukhamedov <2shermux@gmail.com>.

these models, atomic embedding encodes the atomic identifier into vector arrays, which are first initialized randomly and optimized during training.

Despite the increasing use of deep learning in computational chemistry, many aspects of NLP models have yet to be fully explored. One of them is the attention mechanism²⁷, which allows the model to focus on specific parts of the input data when making predictions. It works by assigning different levels of importance, or attention, to different elements in the input sequence. Additionally, the so-called transformer approach has not yet been fully utilized in chemistry. The transformer consists of two distinct components: an encoder responsible for processing the input data and a decoder responsible for generating task-related predictions. In this paper, we introduce a new deep learning model for chemical compounds that utilizes both of these approaches. Specifically, our model incorporates local attention layers to capture properties of local atomic environments and then utilizes a global attention layer to make weighted aggregations of these atomic environment vectors to create a global representation of the entire crystal structure. While the attention mechanism has been previously used in graph neural networks²⁸, this work introduces an atomic representation deep learning model that can be applied to a wide range of tasks. From its components, we call this model 'elEmBERT' (**e**lement **E**mbeddings and **B**idirectional **E**ncoder **R**epresentations from **T**ransformers).

In summary, the main aspects of our work are:

- We use a transformer mechanism for binary classification based on structural information.
- Our model is flexible and can be easily adapted to different types of datasets.
- Benchmarks show the state-of-the-art performance of our model for a variety of material property prediction problems, both involving organic and inorganic compounds.

2 Methods

As input to the neural network (NN), we utilize atomic pair distribution functions (PDFs) and the atom types that compose the compounds. The PDF represents the probability of finding an atom inside a sphere with a radius r centered at a selected atom²⁹. To prepare the training data, we calculate PDFs employing the ASE library³⁰ with a cutoff radius of 10Å. The second input for the NN consists of element embedding vectors. To achieve this, all elements in all crystals are mapped to integers (typically using the nuclear number), creating an elemental vocabulary of size $V_{size}=101$. These embeddings are then passed to the BERT module.

BERT (Bidirectional Encoder Representations from Transformers) is a pre-trained deep learning model originally designed for natural language processing (NLP) tasks. It employs a bidirectional transformer encoder to capture word context in sentences, allowing it to generate accurate text representations. BERT employs masked language modeling (MLM), where some tokens in a sentence are masked or replaced with a [MASK] token, and the model is trained to predict the original word based on the surrounding context. Additionally, BERT uses next sentence prediction, training on pairs of sentences to predict whether the second sentence follows the first.

Our model is illustrated in Fig. 1. It can use various combinations of embedding sizes, encoder-decoder layers, and attention heads. In chemical applications, the atomic composition of a compound can be equated to a sentence, with individual atoms serving as constituent tokens. Leveraging this analogy, we introduce four new tokens to the vocabulary: [MASK] for MLM, [UNK] for unseen tokens, [CLS] for classification, and [SEP] for separating two compounds.

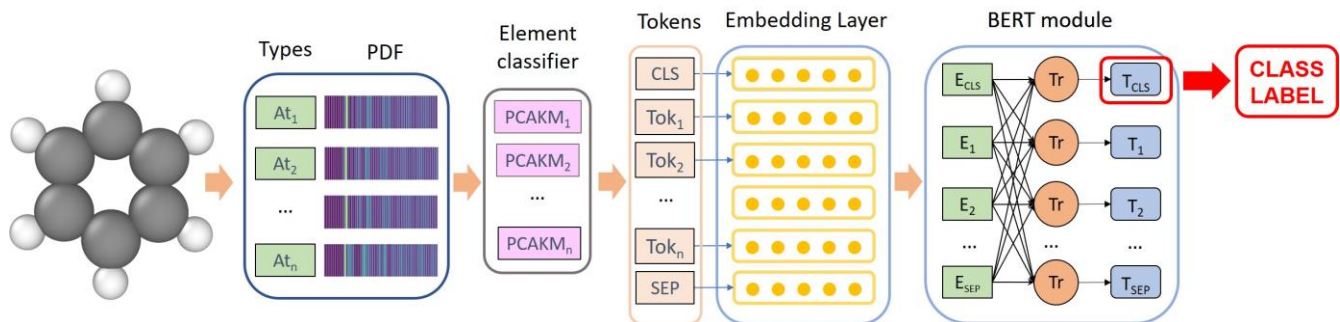


Figure 1. Classification Model Architecture: The initial step involves computing the pair distribution function for each element based on atom positions within the chemical compound. This information is then passed through the PCAKM layer. Subsequently, the resulting subelements are converted into tokens, with additional tokens incorporated before input into the BERT module. The [CLS] token output vector from BERT is used for the classification task.

In a chemical compound, each element can exhibit different oxidation states or formal charges, indicating the relative electron loss or gain during chemical reactions. Considering the foundations of chemistry, it is evident that the elements composing them do not interact uniformly, but instead exhibit specific interactions with neighboring atoms. In the case of inorganic substances, such interactions can manifest themselves as ionic interactions represented by the oxidation state, while for

organic substances, it may be covalent bonding. To create a universal criterion for understanding these interactions, we considered the number of electrons that can participate in a chemical reaction. Using this criterion, we categorized the elements in our training dataset into subelements based on the number of electrons in their outer shell or their oxidation states. However, it is important to note that information about the type of interaction between atoms in molecular structures is often missing, and existing algorithms can be prone to errors. In view of this and recognizing that the length of the chemical bond carries information about the type of interaction, we used Principal Component Analysis (*PCA*) to reduce the dimensionality of PDF vectors. We then employed a k_{means} algorithm to cluster the outputs and categorize elements into subelement classes. This is similar to what has often been done manually when developing classical force fields. Examples of such differentiation are presented in Fig. 2.

We trained an individual model for each element in our dataset, resulting in a total of 192 models, including one *PCA* and one k_{means} model for each element. The final dictionary size was $V_{size}=565$.

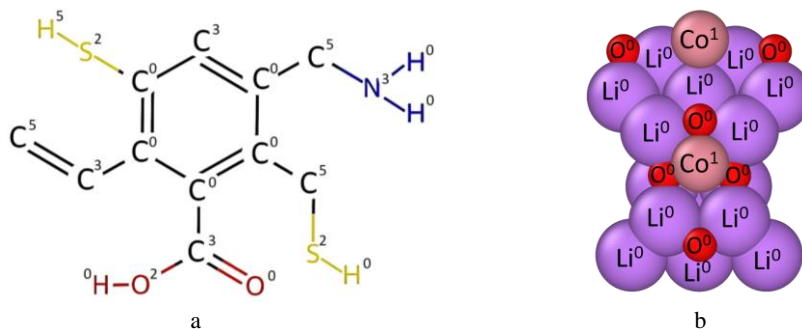


Figure 2. Two examples illustrating the division of elements into sub-elements based on their environment: a hypothetical organic compound (a) and Li_8CoO_6 (b) crystal with ID mp-27920. The numbers at the top right of elements correspond to subelements.

In the following sections, we will present the results of prediction models with specific parameters, including an embedding size of 32, 2 attention heads, and 2 layers. We explored two model versions, V0 (where the *PCA-K_m* block is omitted) and V1, as discussed previously. These calculations were carried out three times for each dataset, using random numbers 12345, 67890, and 234567.

3 Results

We trained our eEmBERT model to perform various classification tasks. To do this, we used the [CLS] token and added an additional layer to the BERT module with the same number of neurons as there are classes in the dataset. Our first task involved using the Materials Project (MP) metallicity dataset to predict the metallicity of materials based on crystal structure information^{31,32}. Next, we employed a portion of the datasets gathered for the CegaNN model³³. This led us to undertake a classification task known as the Liquid-Amorphous (LA) task, which revolves around distinguishing between liquid and amorphous phases of silicon (Si). The LA dataset comprises 2,400 Si structures, evenly divided between amorphous and liquid phases (50% each). Importantly, these Si structures lack symmetry and differ solely in terms of density and coordination number. In addition to these tasks, we evaluated the eEmBERT model's ability to classify material polymorphs across different dimensionalities, specifically clusters (0D), sheets (2D), and bulk structures (3D). Carbon, with its wide range of allotropes spanning these dimensionalities, served as an excellent system for assessing the efficiency of our network model in dimensionality classification (DIM task). The DIM dataset contained 1,827 configurations. Finally, we ventured into characterizing the space group of crystal structures, encompassing a total of 10,517 crystal structures distributed among eight distinct space groups (SG task)³⁴.

Expanding beyond inorganic material datasets, we incorporated organic compounds, which greatly outnumber their inorganic counterparts. This expansion encompasses an extended range of properties, including biochemical and pharmaceutical aspects. To rigorously validate our model, we turned to benchmark datasets from MoleculeNet³⁵, specifically BBBP (Blood-Brain Barrier Penetration), ClinTox (Clinical Toxicity), BACE (β -Secretase), SIDER (Side Effect Resource)³⁶, and Tox21. These datasets cover a diverse array of chemical compounds and provide a comprehensive assessment of our model's predictive performance for binary properties or activities associated with organic molecules. In this context, a positive instance signifies that a molecule possesses a specific property, while a negative instance indicates its absence. The MoleculeNet dataset primarily comprises organic molecules represented in SMILES format. For analysis purposes, we converted these SMILES formulas into the standard XYZ format using the Open Babel software³⁷ and RDKit package³⁸. To evaluate our model's performance, we employed the 'Receiver Operating Characteristic - Area Under the Curve' (ROC-AUC) metric, a common measure for assessing binary classification quality. ROC-AUC quantifies the model's ability to differentiate between positive and negative classes based on predicted probabilities. We divided the datasets into three subsets: the training set, the validation set, and the test set, with an 80:10:10 ratio. The ROC-AUC results reported in Table 1 are based on the test set.

These results serve as a reliable metric for evaluating prediction capabilities and the model's ability to generalize to new instances. Notably, the Tox21 and SIDER datasets encompass 12 and 27 individual tasks, respectively, each corresponding to specific toxicity predictions.

Table 1. Performance of different models applied to datasets (Matbench to TOXIC21) used in this work. A Bold font indicates the best performance and an underline represents the second-best performance, and the last column presents previous results obtained from other models. V0 represents models that use chemical element embeddings, while V1 uses subelement embeddings as input for the BERT module.

Benchmark	V0	V1	BEST
MP metallicity	<u>0.961 ± 0.001</u>	0.965 ± 0.001	0.950 ³⁹
SG	0.944 ± 0.003	<u>0.968 ± 0.002</u>	1 ³³
LA	0.475 ± 0.014	<u>0.980 ± 0.003</u>	1 ³³
DIM	0.893 ± 0.013	<u>0.958 ± 0.003</u>	1 ³³
BACE	0.827 ± 0.005	<u>0.856 ± 0.010</u>	0.888 ⁴⁰
BBBP	0.900 ± 0.020	<u>0.905 ± 0.025</u>	0.932 ⁴⁰
CLINTOX	0.945 ± 0.011	0.951 ± 0.016	<u>0.948</u> ⁴¹
HIV	<u>0.978 ± 0.002</u>	0.979 ± 0.003	0.776 ⁴²
SIDER	0.778 ± 0.032	<u>0.777 ± 0.028</u>	0.659 ⁴⁰
TOX21	0.961 ± 0.006	<u>0.958 ± 0.007</u>	0.860 ⁴¹

Table 1 provides clear evidence that the accuracy of predictions improves as the number of subtypes increases, particularly for inorganic compounds. In the LA task, using single-element inputs, such as Si, results in only 50% accuracy, which is comparable to random guessing. However, incorporating sub-elements significantly enhances the performance, leading to an impressive ROC-AUC of 0.98. Our approach also demonstrates improved accuracy across other datasets. While further increasing the number of sub-elements has a relatively small impact, it still leads to higher accuracy. In the subsequent sections, we will delve into each dataset, from Matbench to Toxic21, and examine the eEmBERT-V1 model in more detail, providing comprehensive insights into the predictions.

MP metallicity

Figure 3a illustrates the confusion matrix and presents the performance of the eEmBERT-V1 model in classifying MP metallicity. In this task, the objective is to predict or estimate whether a material or chemical compound is a metal or not. The dataset for this task comprises 106,113 samples of training structures and 21,222 samples of test structures. Our trained model achieves a binary accuracy of approximately 0.91 and an AUC of 0.965 on the test set.

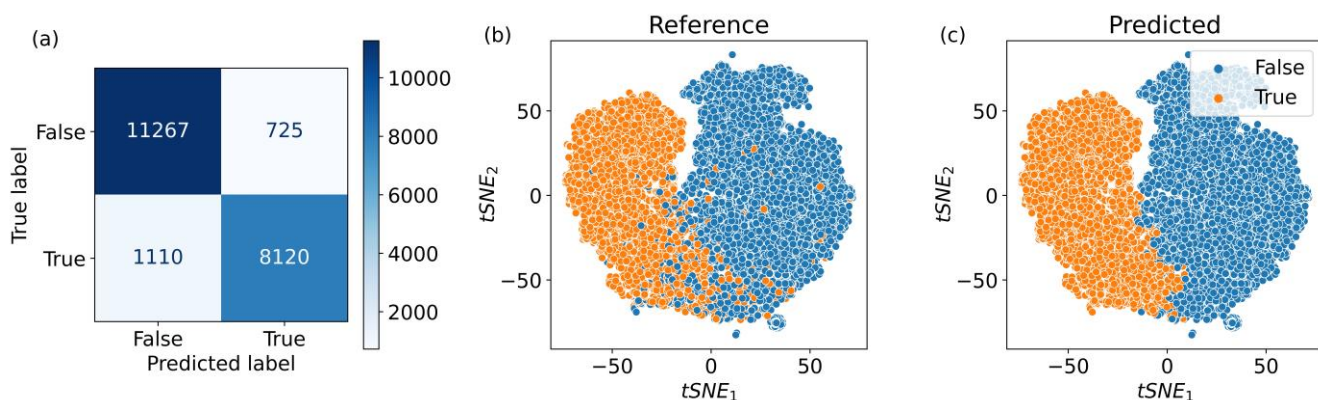


Figure 3. Confusion matrix (a) and visualization of [CLS] token embeddings for the MP metallicity dataset for the reference (b) and predicted (c) datasets: blue circles denote negative labels (not metal) and orange dots represent positive labels (metal).

In Figure 3b, the t-SNE (t-distributed stochastic neighbor embedding) plot shows the embeddings of the entire reference dataset, categorized by labels, revealing a smooth differentiation among labels within the feature space. Figure 3c demonstrates how our model classifies the reference dataset. It is evident that the classification models create a clear separation in the feature space, in contrast to the diffuse boundary in the reference dataset. The primary errors are located at the boundary, where the model sometimes struggles to effectively capture the diffusive behavior. The metallicity prediction task highlights

eLmBERT's remarkable capability to characterize these binary properties of crystals. The achieved accuracy surpasses the capabilities of previously published models, including those of GNNs.

LA, DIM and SG

This section presents the results obtained from benchmarks conducted for the CegaNN model, beginning with a focus on the LA classification task. In Fig. 4a and 4b show the embedding representation of Si structures based on their labels, reduced through the t-SNE algorithm. Our model effectively segregates the structures into distinct clusters, with two clusters clearly corresponding to their respective classes. However, one cluster exhibits intermixing of structures, which challenges accurate recognition by the model.

The confusion matrices shown in Fig. 4c-e provide insights into the performance of the eLmBERT-V1 model across the LA, DIM, and SG datasets. The model achieves a high accuracy of approximately 0.958 on the DIM task's test set and a slightly higher accuracy of 0.968 on the SG dataset. These confusion matrices illustrate the model's ability to identify and categorize each structure accurately. It is worth noting that the model faces challenges in distinguishing the bcc (229) structure from others in the SG dataset. This challenge arises from the structural similarities between the bcc structure and others, resulting in identical geometrical representations unless the orientational order of the particles is considered.

While the CegaNN model achieved 100% efficiency in this benchmark, our model does not reach this level of performance. Nonetheless, it demonstrates strengths in terms of versatility, speed, and simplicity for this benchmark as well.

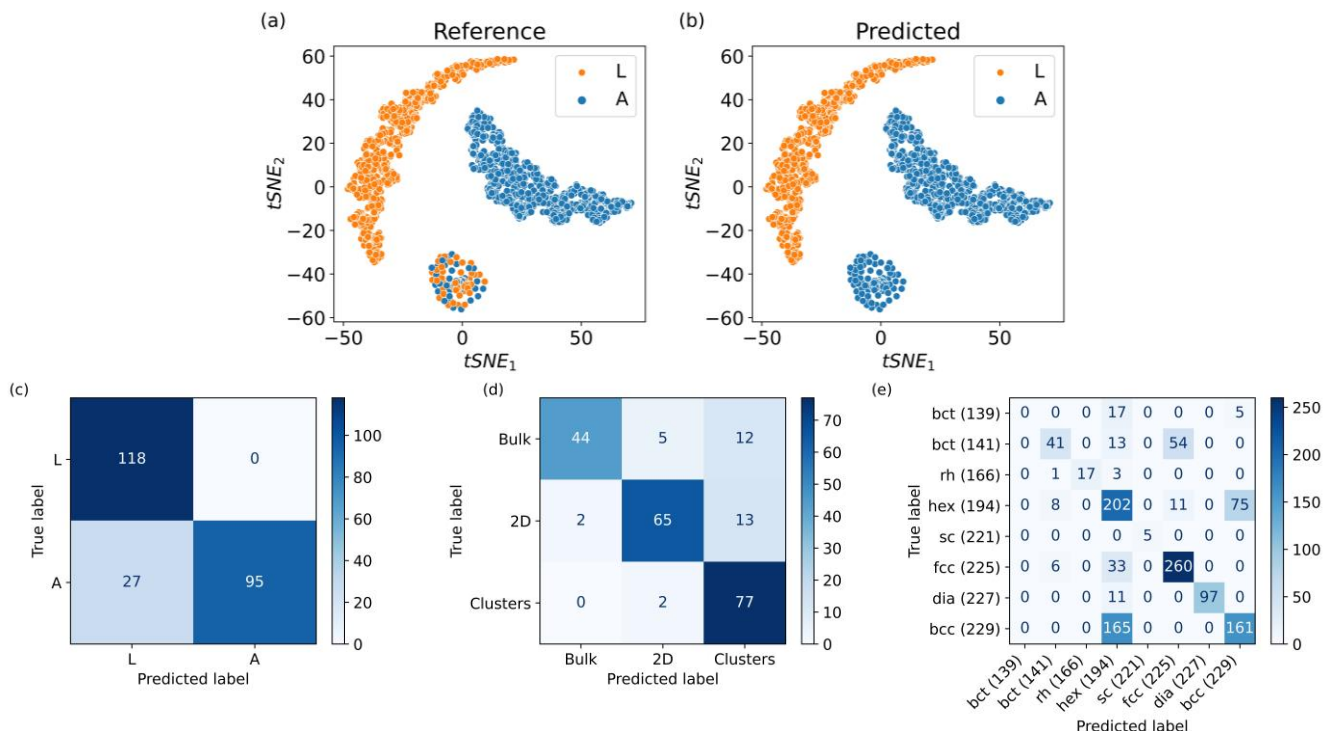


Figure 4. Top row: Visualization of [CLS] Token Embeddings for the LA Dataset: a) reference labels and b) predicted labels. The embeddings are represented using blue circles for liquid phase labels and orange dots for amorphous labels. Bottom row: Confusion matrix analysis of the LA (c), Dim (d), and SG (e) datasets.

BACE

The BACE dataset consists of compounds classified as either active or inactive inhibitors of the β -secretase enzyme, which plays a crucial role in the production of amyloid-beta peptides associated with Alzheimer's disease. This dataset contains a total of 1,513 compounds, including 681 positive instances, making it a valuable resource for developing and evaluating predictive models aimed at identifying potential BACE enzyme inhibitors³⁵.

Our eLmBERT-V1 model, trained on the BACE dataset, achieved a ROC-AUC value of 0.86 in classifying compounds as active or inactive inhibitors. The visualization of our model's predictions on the BACE dataset is presented in Fig. 5. Our model predicts the presence of two distinct clusters, with some infiltration of both labels within each other (Fig. 5c). However, it's important to note that reference labels do not uniformly distribute across these visible clusters; instead, both labels intermixing, leading to errors in both active (true) and inactive (false) predictions. Nevertheless, the attained AUC value of

0.856 closely approximates the best performance obtained from a GNN model. We believe that exploring alternative combinations of model parameters may further enhance these results.

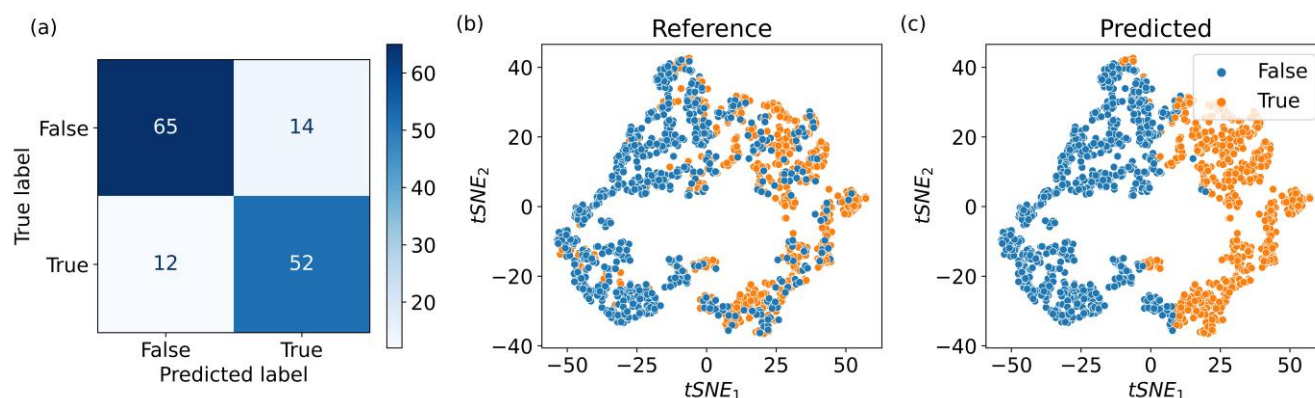


Figure 5. Classification of BACE data: a) Confusion matrix of predicted labels on the test set. b) t-SNE feature representation of the entire reference dataset according to their labels. c) Feature representation of the predicted labels.

BBBP

Next, we used the BBBP dataset, which comprises 2,039 chemical compounds annotated based on their ability to penetrate the blood-brain barrier. This dataset serves as a valuable resource for training and evaluating models aimed at predicting drug candidates' permeability through the blood-brain barrier³⁵. Remarkably, our predictive model achieved a high ROC-AUC value of 0.905, ranking as the second-best value among other models.

As before, we present Fig. 6, which includes the confusion matrix of the test set and t-SNE plots, illustrating the feature representation of labels. As you can see, the model successfully separates compounds according to their labels. However, the primary source of errors again arises from the diffuse boundary, where our model establishes a clear boundary.

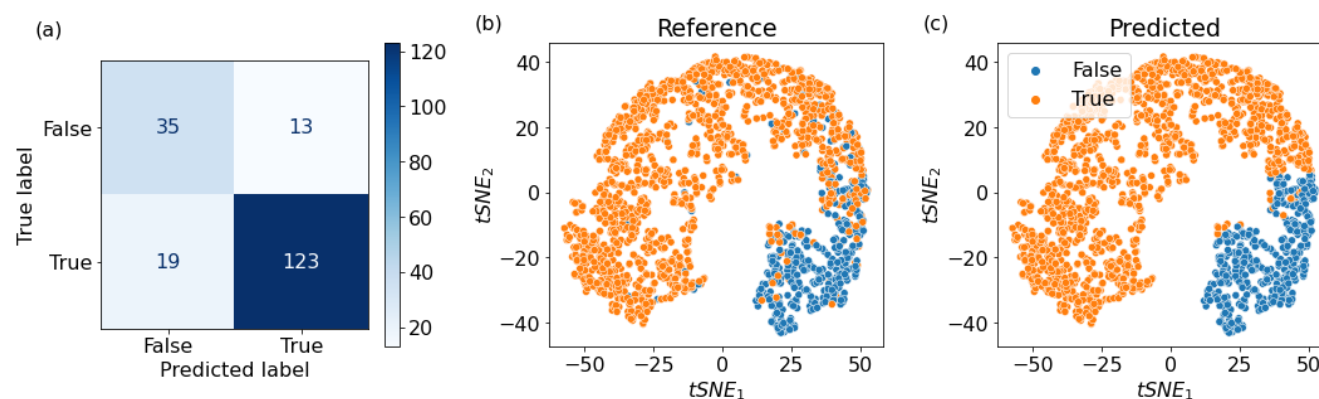


Figure 6. Classification of BBBP data: a) Confusion matrix of predicted labels on the test set. b) t-SNE feature representation of the entire reference dataset according to their labels. c) Feature representation of the predicted labels.

Clintox

The ClinTox dataset is a valuable resource for studying the clinical toxicity profiles of chemical compounds. It provides data on two crucial toxicity endpoints: clinical trial toxicity and FDA approval status. Researchers use this dataset to develop predictive models and evaluate the safety profiles of compounds, aiding in the early identification of potentially toxic substances during the drug development process³⁵. The ClinTox dataset contains 1,491 compounds.

The ClinTox model achieves an impressive ROC-AUC accuracy of approximately 0.951 on the FDA approval task, as demonstrated in Fig. 7. Nevertheless, this dataset features only 94 negative instances, which leads to the confusion matrix showing zero predicted False values. A more detailed analysis of t-SNE projections shows that our model identifies a region with the highest concentration of negative values, yielding accurate true predictions for all points within this limited area. However, the criteria for false selection necessitate greater complexity. We believe that increasing the embedding size, along with attention heads and encoder layers, may further enhance our results.

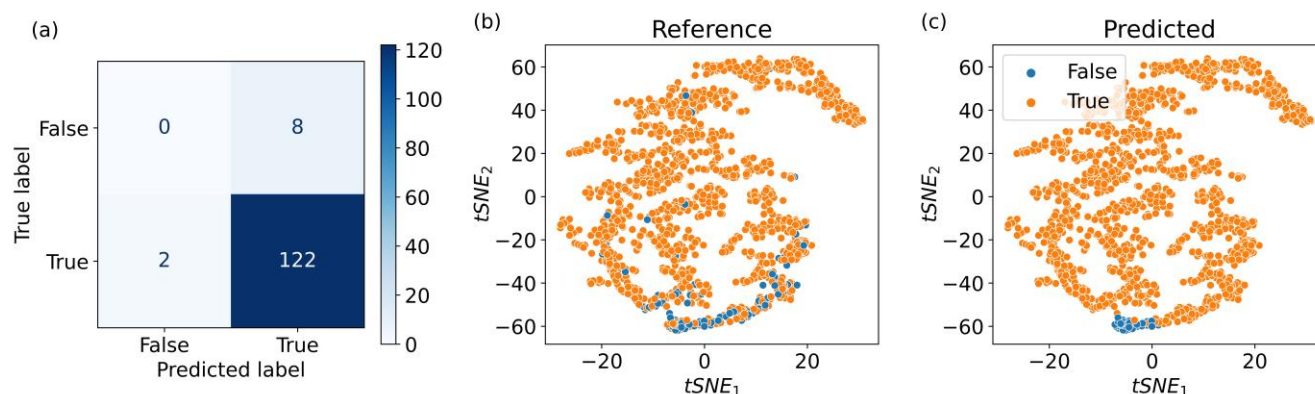


Figure 7. Classification of ClinTox FDA approval task: a) The confusion matrix of predicted labels on the test set. b) The t-SNE feature representation of the entire reference dataset according to their labels. c) The feature representation of the predicted labels.

HIV

The HIV dataset comprises diverse biomedical data related to the Human Immunodeficiency Virus (HIV), including clinical records, genetic sequences, drug resistance profiles, and more. Machine learning techniques are applied to this dataset for tasks such as predicting patient treatment responses, identifying drug resistance mutations, and understanding viral evolution patterns. Within the HIV dataset, there are approximately 41,000 distinct data structures, of which 1,443 are considered positive cases. For the task at hand, the achieved AUC score is an impressive 0.98. Notably, the primary source of erroneous predictions lies in the positive classification of negative compounds, as presented in the confusion matrix plot (Fig. 8a). Fig. 8b illustrates that some positive data points continue to mix with negative ones, contributing to these misclassifications. Furthermore, a diffuse region housing negative values (found in the lower-right region) also contributes to these inaccuracies. Despite the notable occurrence of incorrect positive predictions, it's worth emphasizing that our model demonstrates a robust capability to effectively categorize HIV compounds. Importantly, the highest AUC score achieved by other models remains considerably lower at 0.778, significantly lagging behind our results.

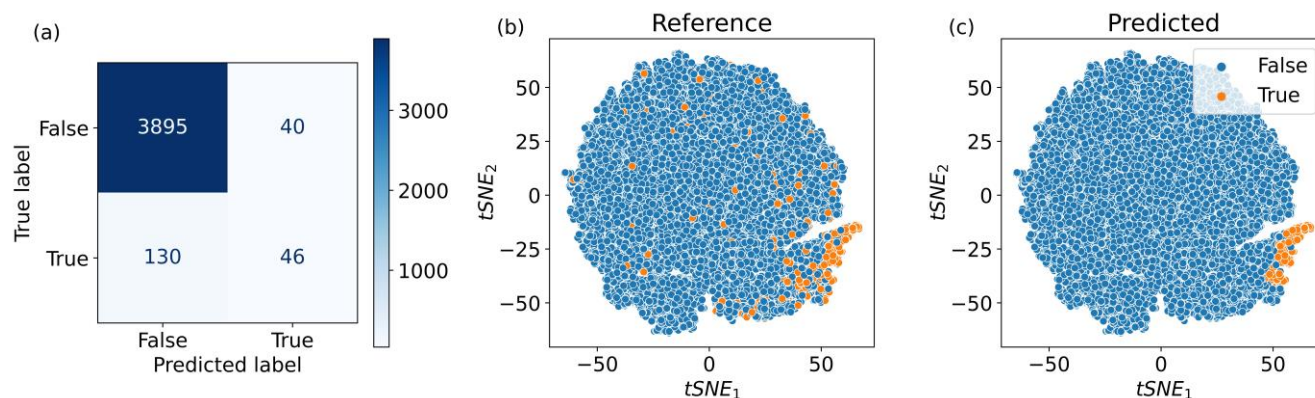


Figure 8. Classification of ClinTox data: a) Confusion matrix of predicted labels on the test set. b) t-SNE feature representation of the entire reference dataset according to their labels. c) Feature representation of the predicted labels.

SIDER

The SIDER dataset serves as a comprehensive pharmacovigilance resource, containing structured information on drug-associated side effects. Curated from diverse sources such as clinical trials, regulatory reports, and medical literature, it offers a systematic compilation of adverse drug reactions associated with various pharmaceutical interventions. The SIDER dataset plays a vital role in assessing drug safety, understanding adverse reaction patterns, and informing clinical decision-making and drug development. It comprises 27 individual tasks, each requiring a corresponding model for fitting. The training results are presented in Table 2, where the average AUC value across all tasks is approximately 0.78. This notably exceeds the previous best-predicted value of 0.659 (over all tasks). The task with the lowest AUC value was the initial SIDER task, concerning Hepatobiliary disorders.

The Meta-MGNN (MMGNN) model achieved a score of 0.763⁴³ for this task, compared to 0.635 in our model. However, in other tasks, our model demonstrates comparability or superiority. The average AUC value across all tasks for our model is higher than the reported value, which averaged the first six tasks in the MMGNN model. In Fig. 9, both the confusion matrix of the test set and t-SNE plots for the compound embeddings are illustrated. These visualizations reveal that labels within the feature space of the reference data are intermingled, necessitating a more intricate model than the one employed in this study for effective label separation. Nonetheless, the model proves better suited for other tasks, providing satisfactory results and improvements over prior predictions.

Table 2. ROC-AUC performances of various models on the SIDER dataset. MMGNN denotes the prior top-performing results⁴³. The last column presents the eEmBERT model's average performance across all tasks. The Bold entries signify the highest performance, while underlined values indicate the second-best performance.

SIDER N	1	2	3	4	5	6	7	8	9	10	11	12	13	14
V0	0.626	0.756	<u>0.972</u>	<u>0.735</u>	<u>0.843</u>	<u>0.736</u>	0.958	0.846	0.775	0.712	<u>0.748</u>	0.930	0.802	0.859
V1	<u>0.635</u>	<u>0.723</u>	0.976	0.700	0.881	0.677	<u>0.957</u>	<u>0.865</u>	<u>0.757</u>	<u>0.662</u>	0.769	<u>0.918</u>	<u>0.785</u>	<u>0.838</u>
MMGNN	0.754	0.693	0.723	0.744	0.817	0.741	-	-	-	-	-	-	-	-
SIDER N	15	16	17	18	19	20	21	22	23	24	25	26	27	Ave
V0	<u>0.841</u>	<u>0.675</u>	<u>0.898</u>	<u>0.812</u>	0.792	<u>0.761</u>	<u>0.843</u>	<u>0.750</u>	<u>0.909</u>	0.669	0.758	<u>0.952</u>	0.798	0.778
V1	0.877	0.732	0.921	0.833	<u>0.781</u>	0.798	0.873	0.781	0.918	<u>0.545</u>	<u>0.726</u>	0.962	<u>0.731</u>	<u>0.777</u>
MMGNN	-	-	-	-	-	-	-	-	-	-	-	-	-	0.747

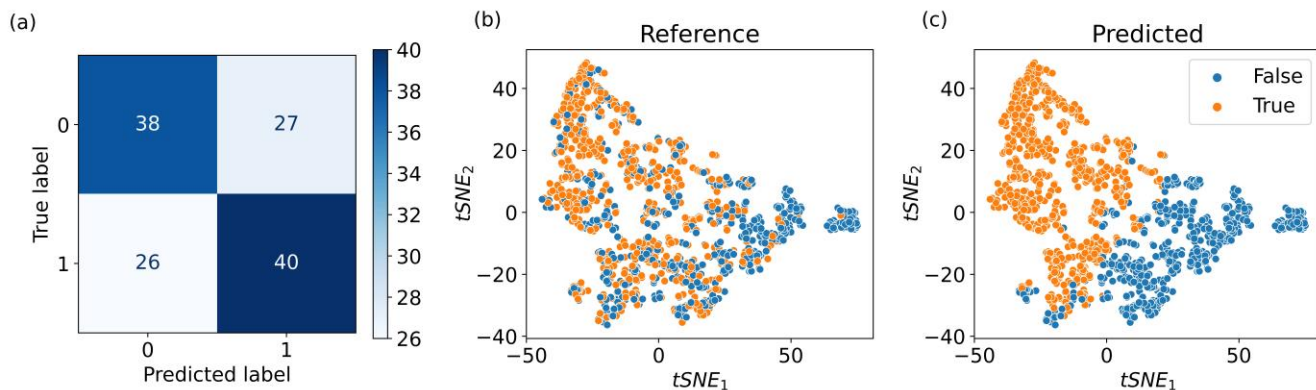


Figure 9. Classification of SIDER-1 data: a) Confusion matrix of predicted labels on the test set. b) t-SNE feature representation of the entire reference dataset according to their labels. c) Feature representation of the predicted labels.

Toxic21

The Toxic21 dataset is a collection of chemical compounds evaluated for their toxicity against a panel of 12 different biological targets. With over 8,000 compounds, it serves as a valuable resource for predicting the toxicity and potential adverse effects of various chemical compounds. Our model, trained on the Toxic21 dataset, demonstrated impressive performance, achieving an average AUC of 0.96 across all 12 toxicity prediction tasks³⁵. The results of these individual tasks are presented in Table 3, enabling a comprehensive evaluation of the model's performance on each toxicity prediction within the Toxic21 dataset.

Comparing our results with those of the MMGNN model highlights the significant advantages of our approach. Fig. 10 shows the confusion matrix of the test set and the t-SNE projection representing the features of the sr-mmp task in the Toxic21 dataset. As shown, our model predicts distinct patterns in the t-SNE projections, with each label value occupying a specific region (Fig. 10b). The molecular embedding visualizations are also available in the MMGNN model report for the sr-mmp task⁴³. In contrast, our feature space exhibits more structure, with positive values being less dispersed across all compounds. Our model primarily has only a few points that are significantly distant from the positive value region. Both eEmBERT models successfully identify the boundary between these two classes and make predictions (Fig. 10c). Errors primarily arise from diffuse boundary regions and points located far from the true cluster. This observation holds true for all tasks within the Toxic21 dataset.

Table 3. ROC-AUC performances of different tasks from the Tox21 dataset. MMGNN denotes the prior top-performing results⁴³. The last column presents the eEmBERT model's average performance across all tasks. The Bold entry signifies the highest performance, while underlined values indicate the second-best performance.

Model	nr-ahr	nr-ar-lbd	nr-arom	nr-ar	nr-er-lbd	nr-er	nr-ppar-g	sr-are	sr-atad5	sr-hse	sr-mmp	sr-p53	Ave
V0	<u>0.947</u>	0.987	0.973	0.982	<u>0.972</u>	<u>0.924</u>	0.991	<u>0.908</u>	<u>0.982</u>	<u>0.975</u>	<u>0.935</u>	0.970	0.961
V1	0.953	<u>0.981</u>	<u>0.972</u>	0.982	0.976	0.930	<u>0.989</u>	0.911	0.984	0.976	0.941	0.970	<u>0.958</u>
MMGNN	-	-	-	-	-	-	-	-	-	0.748	0.804	0.790	0.781

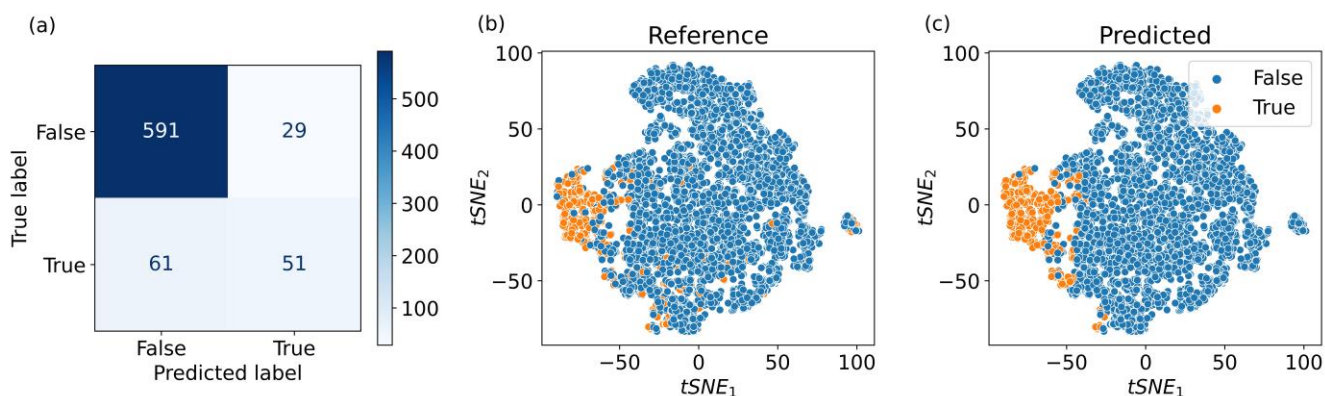


Figure 10. Classification of sr-mmp data from Tox21 dataset: a) Confusion matrix of predicted labels on the test set. b) t-SNE feature representation of the entire reference dataset according to their labels. c) Feature representation of the predicted labels.

The binary classification results of our model for organic compounds exemplify its exceptional efficiency in predicting the behavior of interactions between organic compounds and protein molecules. By accurately classifying these compounds, our model provides valuable insights into their potential effects and interactions within biological systems. This capability holds significant promise for drug discovery, as it enables the identification of organic compounds that have a high likelihood of binding to specific protein targets and exerting desired therapeutic effects.

4 Conclusions

In conclusion, the deep learning model presented in this paper signifies a significant advancement in the application of machine learning to computational chemistry. By integrating the attention mechanism and a transformer-based approach, our model can capture both local and global properties of chemical compounds, enabling highly accurate predictions of chemical properties that outperform similar approaches. Our innovative combination of principal component analysis and k-means clustering for sub-elements accounts for the nuanced effects stemming from electronic structure, a fact confirmed through the analysis of numerous chemical databases. Our classification approach, which relies on compound embeddings, has substantially improved prediction accuracy compared to previously published scores. Additionally, t-SNE projections provide valuable insights into the classification mechanisms and can pinpoint sources of erroneous predictions. Beyond accurately predicting desired properties, we believe that our model has the potential to illuminate the underlying reasons behind structure/property relationships.

Acknowledgements

The work has partially been carried out within the framework of the EUROfusion Consortium and received funding from the Euratom research and training programme by Grant Agreement No. 101052200-EUROfusion. SS has received funding from the European Union's Horizon 2020 research and innovation programme under the Marie Skłodowska-Curie Grant Agreement No. 847476. The views and opinions expressed herein do not necessarily reflect those of the European Commission. The computational results have been obtained using the HPC infrastructure LEO of the University of Innsbruck.

Data availability

All data used in this paper are publicly available and can be accessed from various sources. The structure files for the MP metallicity dataset are accessible at <https://matbench.materialsproject.org/>. The LA, SG, and DIM datasets are available at <https://github.com/sbanik2/CEGANN/tree/main/pretrained>. The BACE, BBBP, Clintox, HIV, and SIDER datasets can be retrieved from <https://moleculenet.org/>. Structure files for the Tox21 dataset can be obtained from

<https://tripod.nih.gov/tox21/challenge/data.jsp>. The source code used in this study is available at <https://github.com/dmamur/elembert>, and detailed Python notebooks for replicating all calculations can be found on the corresponding GitHub page.

References

1. Ng, M.-F., Zhao, J., Yan, Q., Conduit, G. J. & Seh, Z. W. Predicting the state of charge and health of batteries using data-driven machine learning. *Nat. Mach. Intell.* **2**, 161–170 (2020).
2. Liu, Y., Guo, B., Zou, X., Li, Y. & Shi, S. Machine learning assisted materials design and discovery for rechargeable batteries. *Energy Storage Mater.* **31**, 434–450 (2020).
3. Sawant, V., Deshmukh, R. & Awati, C. Machine learning techniques for prediction of capacitance and remaining useful life of supercapacitors: A comprehensive review. *J. Energy Chem.* **77**, 438–451 (2023).
4. Iwasaki, Y. *et al.* Machine-learning guided discovery of a new thermoelectric material. *Sci. Rep.* **9**, 1–7 (2019).
5. Akhter, M. N., Mekhilef, S., Mokhlis, H. & Shah, N. M. Review on forecasting of photovoltaic power generation based on machine learning and metaheuristic techniques. *IET Renew. Power Gener.* **13**, 1009–1023 (2019).
6. Toyao, T. *et al.* Machine Learning for Catalysis Informatics: Recent Applications and Prospects. *ACS Catal.* **10**, 2260–2297 (2020).
7. Vamathevan, J. *et al.* Applications of machine learning in drug discovery and development. *Nat. Rev. Drug Discov.* **18**, 463–477 (2019).
8. Mikolov, T., Chen, K., Corrado, G. & Dean, J. Efficient estimation of word representations in vector space. *1st Int. Conf. Learn. Represent. ICLR 2013 - Work. Track Proc.* 1–12 (2013).
9. Tshitoyan, V. *et al.* Unsupervised word embeddings capture latent knowledge from materials science literature. *Nature* **571**, 95–98 (2019).
10. Hansen, K. *et al.* Machine learning predictions of molecular properties: Accurate many-body potentials and nonlocality in chemical space. *J. Phys. Chem. Lett.* **6**, 2326–2331 (2015).
11. Jaeger, S., Fulle, S. & Turk, S. Mol2vec: Unsupervised Machine Learning Approach with Chemical Intuition. *J. Chem. Inf. Model.* **58**, 27–35 (2018).
12. Goh, G. B., Hodas, N. O., Siegel, C. & Vishnu, A. SMILES2Vec: An Interpretable General-Purpose Deep Neural Network for Predicting Chemical Properties. (2017) doi:10.475/123.
13. Zhang, Y. F. *et al.* SPVec: A Word2vec-Inspired Feature Representation Method for Drug-Target Interaction Prediction. *Front. Chem.* **7**, 1–11 (2020).
14. Stanev, V. *et al.* Machine learning modeling of superconducting critical temperature. *npj Comput. Mater.* **4**, (2018).
15. Chen, C., Ye, W., Zuo, Y., Zheng, C. & Ong, S. P. Graph Networks as a Universal Machine Learning Framework for Molecules and Crystals. *Chem. Mater.* **31**, 3564–3572 (2019).
16. Kong, S. *et al.* Density of states prediction for materials discovery via contrastive learning from probabilistic embeddings. *Nat. Commun.* **13**, 1–12 (2022).
17. Gori, M., Monfardini, G. & Scarselli, F. A new model for learning in graph domains. *Proc. Int. Jt. Conf. Neural Networks* **2**, 729–734 (2005).
18. Zhang, S., Liu, Y. & Xie, L. Molecular Mechanics-Driven Graph Neural Network with Multiplex Graph for Molecular Structures. 1–14 (2020).
19. Shui, Z. & Karypis, G. Heterogeneous molecular graph neural networks for predicting molecule properties. *Proc. - IEEE Int. Conf. Data Mining, ICDM 2020-Novem*, 492–500 (2020).
20. Fung, V., Zhang, J., Juarez, E. & Sumpter, B. G. Benchmarking graph neural networks for materials chemistry. *npj Comput. Mater.* **7**, 1–8 (2021).
21. Xie, T. & Grossman, J. C. Crystal Graph Convolutional Neural Networks for an Accurate and Interpretable

- Prediction of Material Properties. *Phys. Rev. Lett.* **120**, (2018).
22. Bartók, A. P., Kondor, R. & Csányi, G. On representing chemical environments. *Phys. Rev. B - Condens. Matter Mater. Phys.* **87**, 1–16 (2013).
 23. Huo, H. & Rupp, M. Unified Representation of Molecules and Crystals for Machine Learning. *Mach. Learn. Sci. Technol.* **3**, 045017 (2022).
 24. Behler, J. Four Generations of High-Dimensional Neural Network Potentials. *Chem. Rev.* **121**, 10037–10072 (2021).
 25. Schütt, K. T. *et al.* SchNet: A continuous-filter convolutional neural network for modeling quantum interactions. *Adv. Neural Inf. Process. Syst.* **2017-December**, 992–1002 (2017).
 26. Unke, O. T. & Meuwly, M. PhysNet: A Neural Network for Predicting Energies, Forces, Dipole Moments, and Partial Charges. *J. Chem. Theory Comput.* **15**, 3678–3693 (2019).
 27. Vaswani, A. *et al.* Attention is all you need. *Adv. Neural Inf. Process. Syst.* **2017-Decem**, 5999–6009 (2017).
 28. Louis, S. Y. *et al.* Graph convolutional neural networks with global attention for improved materials property prediction. *Phys. Chem. Chem. Phys.* **22**, 18141–18148 (2020).
 29. Billinge, S. J. L. The rise of the X-ray atomic pair distribution function method: A series of fortunate events. *Philos. Trans. R. Soc. A Math. Phys. Eng. Sci.* **377**, (2019).
 30. Hjorth Larsen, A. *et al.* The atomic simulation environment—a Python library for working with atoms. *J. Phys. Condens. Matter* **29**, 273002 (2017).
 31. Jain, A. *et al.* Commentary: The materials project: A materials genome approach to accelerating materials innovation. *APL Mater.* **1**, (2013).
 32. Ong, S. P. *et al.* The Materials Application Programming Interface (API): A simple, flexible and efficient API for materials data based on REpresentational State Transfer (REST) principles. *Comput. Mater. Sci.* **97**, 209–215 (2015).
 33. Banik, S. *et al.* CEGANN: Crystal Edge Graph Attention Neural Network for multiscale classification of materials environment. *npj Comput. Mater.* **9**, 1–12 (2023).
 34. Ziletti, A., Kumar, D., Scheffler, M. & Ghiringhelli, L. M. Insightful classification of crystal structures using deep learning. *Nat. Commun.* **9**, 1–10 (2018).
 35. Wu, Z. *et al.* MoleculeNet: A benchmark for molecular machine learning. *Chem. Sci.* **9**, 513–530 (2018).
 36. Kuhn, M., Letunic, I., Jensen, L. J. & Bork, P. The SIDER database of drugs and side effects. *Nucleic Acids Res.* **44**, D1075–D1079 (2016).
 37. O’Boyle, N. M. *et al.* Open Babel. *J. Cheminform.* **3**, 1–14 (2011).
 38. RDKit: Open-source cheminformatics. <https://www.rdkit.org>.
 39. Chen, C. & Ong, S. P. AtomSets as a hierarchical transfer learning framework for small and large materials datasets. *npj Comput. Mater.* **7**, (2021).
 40. Li, Y. *et al.* GLAM: An adaptive graph learning method for automated molecular interactions and properties predictions. *Nat. Mach. Intell.* **4**, 645–651 (2022).
 41. Li, P. *et al.* TrimNet: learning molecular representation from triplet messages for biomedicine. *Brief. Bioinform.* **22**, bbaa266 (2021).
 42. Baek, J., Kang, M. & Hwang, S. J. Accurate Learning of Graph Representations with Graph Multiset Pooling. **1**, 1–22 (2021).
 43. Guo, Z. *et al.* Few-shot graph learning for molecular property prediction. *Web Conf. 2021 - Proc. World Wide Web Conf. WWW 2021* 2559–2567 (2021) doi:10.1145/3442381.3450112.